Observation of the Fermionic Joule-Thomson Effect

Yunpeng Ji,[1,*] Jianyi Chen,[1] Grant L. Schumacher,[1] Gabriel G. T. Assumpção,[1]
Songtao Huang,[1] Franklin J. Vivanco,[1] and Nir Navon[1,2]
[1]Department of Physics, Yale University, New Haven, Connecticut 06520, USA
[2]Yale Quantum Institute, Yale University, New Haven, Connecticut 06520, USA

(Received 23 May 2023; revised 14 November 2023; accepted 9 January 2024; published 11 April 2024)

We report the first observation of the quantum Joule-Thomson (JT) effect in ideal and unitary Fermi gases. We study the temperature dynamics of these systems while they undergo an energy-per-particle conserving rarefaction. For scale-invariant systems, whose equations of state satisfy the relation $U \propto PV$, this rarefaction conserves the specific enthalpy, which makes it thermodynamically equivalent to a JT throttling process. We observe JT heating in an ideal Fermi gas, a direct consequence of Pauli blocking. In a unitary Fermi gas, we observe that the JT heating is marginal in the temperature range $0.2 \lesssim T/T_F \lesssim 0.8$ as the repulsive quantum-statistical effect is lessened by the attractive interparticle interactions.

DOI: 10.1103/PhysRevLett.132.153402

The Joule-Thomson (JT) effect is a fundamental phenomenon in thermodynamics whereby the temperature T of a thermally isolated system changes in response to a decrease of the pressure P while the specific enthalpy h is conserved. This effect has played a momentous role in the history of thermodynamics [1] and the birth of modern cryogenics [2]. In its own right, the JT effect has attracted interest as a probe of the thermodynamics of imperfect (i.e. interacting) gases [3,4] and, more recently, in relation to black hole expansion dynamics [5–7].

In classical gases, the JT effect is tied to interparticle interactions. This can be illustrated with a simple equation of state (EOS) $PV = Nk_BT + a_{\mathrm{int}}N^2/V$, i.e., the Van der Waals EOS without the excluded-volume effect; N is the number of particles, V is the volume, and a_{int} is an interaction parameter that is positive for repulsive interactions and negative for attractive ones. In the limit of weak interactions ($a_{\mathrm{int}}N/V \ll k_BT$), the Joule-Thomson coefficient $\mu_{\mathrm{JT}} \equiv (\partial T/\partial P)_h$ is $\mu_{\mathrm{JT}} \propto -a_{\mathrm{int}}/c_P$ in this model ($c_P > 0$ is the specific heat); thus the system heats (respectively cools) in the case of repulsive (respectively attractive) interactions.

Surprisingly, the JT effect does not require interactions. Indeed, shortly after the discovery of quantum indistinguishability, it was predicted that quantum correlations give rise to a nontrivial JT effect even in the absence of interactions [8]; in essence, Bose-Einstein particles would behave as if they were classically attracting and Fermi-Dirac particles as if they were repelling. The opposite nature of these respective quantum JT effects originate from profoundly different microscopic physics: at low temperatures, the former is driven by the Bose saturation of the single-particle excited states [9], while the latter, by Fermi hole heating [10]. Despite being a fundamental prediction of quantum statistical mechanics, only recently has the bosonic JT effect been observed [11], whereas the fermionic one has remained elusive.

In this work we measure the JT effect in Fermi systems. In the textbook presentation of the JT process, a gas is throttled through a porous plug from a high-P to a low-P compartment [see sketch in Fig. 1(a)]. In our experiment, we realize a JT rarefaction either by exploiting collisions with high-energy particles from the residual background gas (in the vacuum chamber) or by controllably transferring atoms into internal states that are essentially not interacting with the states of interest [Fig. 1(b)]. In either case, the loss process is independent of the energy per particle $u = U/N$ where U is the total internal energy. For a scale-invariant gas, whose EOS satisfies $U \propto PV$, this process is thermodynamically equivalent to a JT one.

We first focus on the JT effect in the ideal Fermi gas. We prepare weakly interacting spin-1/2 Fermi gases of ^{6}Li atoms in a balanced mixture of the first and third lowest Zeeman sublevels (respectively labeled $|1\rangle$ and $|3\rangle$). Our gases are confined in optical boxes so that their density and other thermodynamics quantities are spatially uniform, making the interpretation of our measurements straightforward [12,13]. Our cylindrical boxes have a radius $R = 77(2)$ μm and an adjustable length L between 58 μm and 120 μm [see an example of a box in Figs. 1(b) and 1(c)]. The samples are evaporated at a bias magnetic field $B = 287$ G, where the s-wave scattering length is $a \approx -880a_0$ (a_0 is the Bohr radius). The B field is then ramped to its final value, where levitation against gravity is done with a magnetic field gradient; the difference of magnetic moments of the trapped states used in this work (<0.8%) is negligible for our experimental parameters. We typically start our experiments with a degenerate spin-1/2 Fermi gas, $T \lesssim E_F/k_B$ (where $E_F = \hbar^2/(2m)(6\pi^2N/V)^{2/3}$ is the Fermi energy); henceforth, all thermodynamic quantities (such

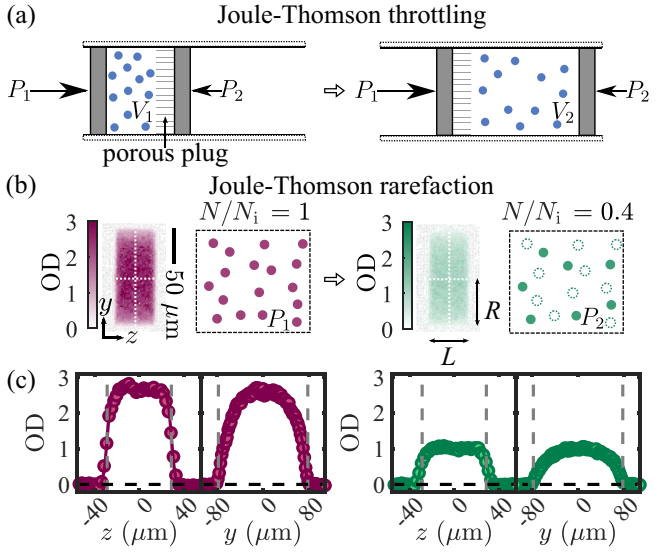

FIG. 1. Joule-Thomson rarefaction of a homogeneous Fermi gas. (a) Classic throttling process. A thermally isolated gas is forced from a high pressure chamber (left) to a low pressure one (right). (b) JT process through a rarefaction at fixed energy per particle u and volume V; N_i is the initial particle number. The images to the left of the cartoons are *in situ* optical density (OD) images of homogeneous Fermi gases of ^{6}Li atoms, before (left, purple) and after (right, green) rarefaction. (c) Cuts along the white dotted lines on the OD images. The solid lines are fits to extract the box volume. The length and radius of this cylindrical box are $L = 58(1)$ μm and $R = 77(2)$ μm, and remain essentially unchanged during rarefaction (see vertical dashed gray lines as guides to the eye, located at the same positions between the left and right panels). The density cuts are colored according to panel (b).

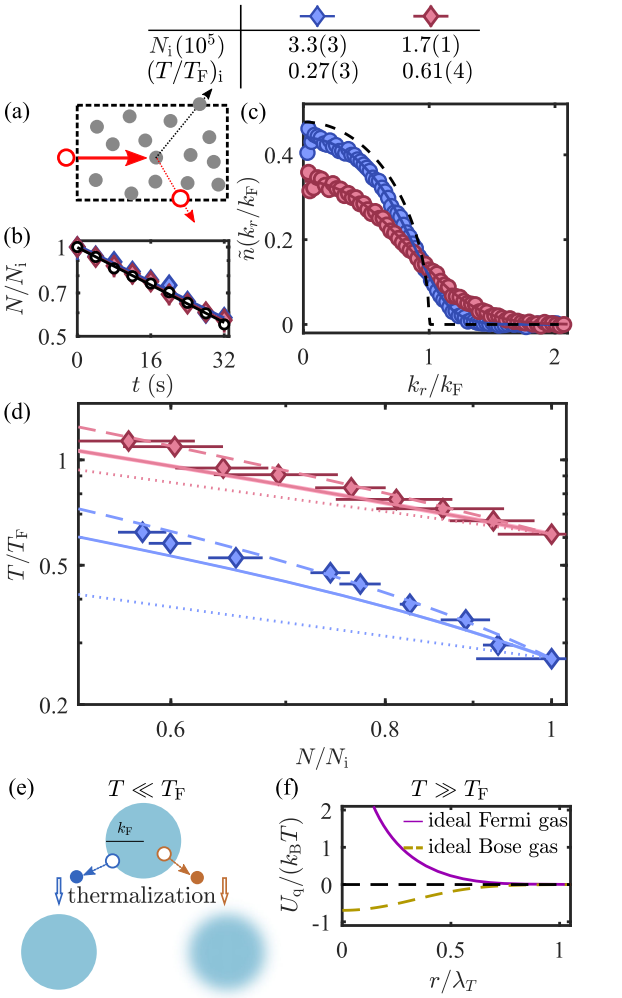

FIG. 2. Joule-Thomson effect of the ideal Fermi gas. (a) Sketch of an energy-independent atom loss due to collisions with high-energy background particles (red empty circle). (b) Decay of a noninteracting Fermi gas (black circles) and weakly interacting Fermi gases (colored diamonds) at different initial T/T_F (see legend). The solid lines are exponential fits. The same marker color is used in (c) and (d). (c) Azimuthally averaged radial momentum distribution of Fermi gases extracted from column integrated OD after a time-of-flight expansion of duration t_{TOF}. The distributions are normalized such that $\int \tilde{n}(k_r/k_F)(2\pi k_r/k_F)\mathrm{d}(k_r/k_F)=1$; here $k_r=m\sqrt{y^2+z^2}/(\hbar t_{TOF})$ and k_F is the Fermi wave number. The distributions correspond to the initial points in (b). The solid lines are fits to Fermi-Dirac distributions to extract temperatures. The black dashed line shows the momentum distribution at $T = 0$. (d) Temperature evolution of weakly interacting Fermi gases during a JT rarefaction. The solid lines are theoretical predictions fixing $(T/T_F)_i$ to the experimentally measured values, with the (barely visible) bands representing the uncertainty on $(T/T_F)_i$. The dashed lines take into account the effect of technical heating in the box (see text and [14]). The dotted lines show the evolution of T/T_F at constant T. (e) Sketch of Fermi hole heating at $T \ll T_F$. The blue (respectively brown) point represents a particle whose removal causes no temperature change (respectively causes heating). (f) Quantum-statistical interaction potential U_q of ideal quantum gases in the high-T limit.

as U, N, etc.) are defined for each spin population. We typically have $N_1 \approx N_3 \approx 8 \times 10^5$, corresponding to a Fermi temperature of $T_F = E_F/k_B \approx 300$ nK.

We take advantage of the slow one-body losses due to collisions with the background gas to realize u-constant rarefactions [Fig. 2(a)], as in [11]. Here, the tunability of interparticle interactions is important as the interactions must obey conflicting requirements. On the one hand, interactions must be weak enough so that we probe essentially ideal gas physics and that $PV \approx (2/3)U$; furthermore, two-body energy-dependent evaporation must be suppressed on the (long) timescale of the measurements. On the other hand, interactions must be strong enough to ensure that the gas is in thermal equilibrium when the measurements are done.

Consequently, we satisfy those conditions by choosing the final value of B such that a is in the range $100a_0 \lesssim a \lesssim 220a_0$. The specific value is picked as large as possible, while ensuring that the decay time is indistinguishable from the vacuum-limited lifetime. In Fig. 2(b), we show examples of decays at various quantum degeneracies (colored diamonds); each data set is normalized to the initial atom number N_i. The lifetimes in those data

series are indistinguishable from that of a noninteracting gas ($|a| \leq 50a_0$), $\tau_{\mathrm{vac}} = 55(2)$ s (see the black circles, the vacuum-limited lifetime in our chamber). At the same time, the two-body elastic collision rate is in the appropriate regime $\Gamma_{\mathrm{el}} \gg 1/\tau_{\mathrm{vac}}$ (in our range of densities and temperatures, $\Gamma_{\mathrm{el}} \geq 0.17\ \mathrm{s}^{-1}$). Furthermore, for our regime of interactions and temperatures, h changes less than 0.01% during the decay, making this rarefaction an excellent approximation of a JT process [14].

We perform thermometry using time-of-flight expansions (see Appendix A and [14]). We show in Fig. 2(c) the momentum distributions for two initial conditions $(T/T_{\mathrm{F}})_{\mathrm{i}} = 0.27(3)$ (blue) and $(T/T_{\mathrm{F}})_{\mathrm{i}} = 0.61(4)$ (red). In Fig. 2(d), we show the temperature dynamics of the gas during rarefaction for these two cases; we plot T/T_{F} versus N/N_{i}, where the instantaneous T_{F} decreases as the gas rarefies. The dotted lines correspond to $T/T_{\mathrm{F}} \propto (N/N_{\mathrm{i}})^{-2/3}$, the expectation for constant-T rarefactions. The measurements show heating, and the main qualitative feature is that the heating is more pronounced for a more quantum-degenerate gas, i.e., the fractional change of T is larger at low T/T_{F} for the same decrease of N/N_{i}.

Quantitatively, we describe the temperature dynamics during this JT process using the dimensionless coefficient $\theta_{\mathrm{JT}} \equiv [\partial \log(T)/\partial \log(P)]_h$. This coefficient is related to the JT coefficient: $\mu_{\mathrm{JT}} = (T/P)\theta_{\mathrm{JT}}$. For a homogeneous gas whose EOS is universal, i.e. for which $P\lambda_T^3/(k_{\mathrm{B}}T)$ only depends on the chemical potential μ and $k_{\mathrm{B}}T$ via the ratio $\mu/(k_{\mathrm{B}}T)$, θ_{JT} is a function of T/T_{F} alone (λ_T is the thermal wavelength). The evolution of T/T_{F} follows $[\partial \log(T/T_{\mathrm{F}})/\partial \log(N)]_h = \theta_{\mathrm{JT}} - 2/3$ [14]. In Fig. 2(d), the solid lines are the theoretical predictions derived from the EOS of the ideal Fermi gas (where $(T/T_{\mathrm{F}})_{\mathrm{i}}$ is fixed to the experimental value). We find good agreement with the data. The small discrepancy is well accounted for by a weak technical heating in our box; the dashed lines show the theoretical predictions from the model $\mathrm{d}\log(T/T_{\mathrm{F}})/\mathrm{d}\log(N) = (\theta_{\mathrm{JT}} - 2/3)(1 + (3/2)\gamma_{\mathrm{tech}}\tau_{\mathrm{vac}}/u)$, where our heating rate $\gamma_{\mathrm{tech}} = 0.58(7)k_{\mathrm{B}} \times \mathrm{nK/s}$ is characterized independently [14].

In the low- and high-T limits, simple pictures provide insights into the microscopic origin of the JT effect. First, for $T \ll T_{\mathrm{F}}$, the state of the gas is essentially a Fermi sea [Fig. 2(e)]. In that case, the average energy per particle lost in a random (energy-independent) removal is only $u_{\mathrm{loss}} \approx (3/5)E_{\mathrm{F}}$; the energy per particle that needs to be removed to keep the temperature constant, $u_T \equiv (\partial U/\partial N)_{T,V}$, is $u_T \approx E_{\mathrm{F}}$. As a result, the system heats up, a process referred to as Fermi hole heating [10].

The interpretation of quantum correlations as statistical "forces" demystifies the quantum JT effect in the $T \gg T_{\mathrm{F}}$ limit. For that purpose, it is useful to consider the pair density correlation function $G(\mathbf{r}_1, \mathbf{r}_2) \equiv \langle \Psi^\dagger(\mathbf{r}_1)\Psi^\dagger(\mathbf{r}_2)\Psi(\mathbf{r}_2)\Psi(\mathbf{r}_1)\rangle / [n(\mathbf{r}_1)n(\mathbf{r}_2)]$, where $\Psi^\dagger(\mathbf{r}_j)$ ($\Psi(\mathbf{r}_j)$) is the field operator that creates (annihilates) a particle at position $\mathbf{r}_j$, and $n(\mathbf{r}_j) \equiv \langle \Psi^\dagger(\mathbf{r}_j)\Psi(\mathbf{r}_j)\rangle$. For an ideal homogeneous gas in the high-T (virial) limit, $G(\mathbf{r}_1,\mathbf{r}_2) = G(r) \approx 1 + \eta \exp(-2\pi r^2/\lambda_T^2)$, where $r = |\mathbf{r}_1 - \mathbf{r}_2|$, $\eta = 1$ for bosons and $\eta = -1$ for fermions ($\eta = 0$ for the classical ideal gas) [20]. For a dilute classical gas, $G(r) \approx \exp[-U_{\mathrm{int}}(r)/(k_{\mathrm{B}}T)]$, where $U_{\mathrm{int}}(r)$ is the interparticle interaction potential. By analogy, one can define an effective quantum-statistical interaction between indistinguishable noninteracting particles, $U_{\mathrm{q}}(r) \equiv -k_{\mathrm{B}}T \log G(r)$ [21,22]. The potential $U_{\mathrm{q}}(r)$ is shown as yellow and purple lines in Fig. 2(f); as intuitively expected, fermions effectively "repel" while bosons "attract" each other. Furthermore, the signs of their quantum JT coefficients are consistent with their respective quantum-statistical interaction [14,23].

We now turn to the unitary Fermi gas, for which $1/a = 0$. Crucially, because $PV - (2/3)U \propto \mathcal{I}/a$, where $\mathcal{I}$ is Tan's contact [24], the universal relation $PV = (2/3)U$ also holds for the unitary gas. This makes the unitary case another special point in the BEC-BCS crossover [25] for which a u-constant rarefaction is also a JT process. We create a unitary gas by preparing a spin-balanced mixture of atoms in states $|1\rangle$ and $|3\rangle$ that is evaporatively cooled and loaded into the optical box at $B \approx 796$ G. The field is then ramped to the Feshbach resonance, $B \approx 690$ G. At this stage we typically have $N_1 \approx N_3 \approx 3 \times 10^5$ at $T/T_{\mathrm{F}} \approx 0.2$ (slightly above the superfluid transition temperature T_{c} [25]).

Just as in the ideal gas case, the two main ingredients to observe the JT effect in this setting are the realization of a u-constant rarefaction and a thermometry method. Both present new challenges compared to the weakly interacting case.

As the collision rate in the unitary gas is so high (typically $\Gamma_{\mathrm{el}}^{\mathrm{uni}} \geq 500\ \mathrm{s}^{-1}$ in our case), the evaporation rate is vastly higher than in the weakly interacting case, threatening the JT nature of the rarefaction. In our deepest box ($U_{\mathrm{box}} \gtrsim 8E_{\mathrm{F}}$), the lifetime of our unitary gas is $\tau_{\mathrm{uni}} \approx 30$ s, close to but a little shorter than τ_{vac} [26] (possibly limited by a slow residual evaporation). To mitigate this issue, we artificially increase the u-independent "loss" rate by applying a weak two-tone microwave pulse of duration $t_{\mu\mathrm{w}}$ to transfer atoms to higher Zeeman sublevels [see Appendix B and Fig. 3(a)]. Measuring the number of atoms remaining in $|1\rangle$ and $|3\rangle$, we find exponential decays with respective characteristic times $\tau_{\mu\mathrm{w}} = 0.33(1)$ s and $\tau_{\mu\mathrm{w}} = 0.35(1)$ s [pink and blue diamonds in Fig. 3(b)]. This timescale is such that $\tau_{\mathrm{uni}} \gg \tau_{\mu\mathrm{w}} \gg 1/\Gamma_{\mathrm{el}}^{\mathrm{uni}}$, i.e. the microwave-induced rarefaction is slow compared to the elastic collision rate so that the gas remains in thermal equilibrium, but fast enough so that energy-dependent losses are negligible. We validate our microwave-induced rarefaction method on the now-verified case of the weakly interacting gas; the effect of the technical heating is now negligible because the

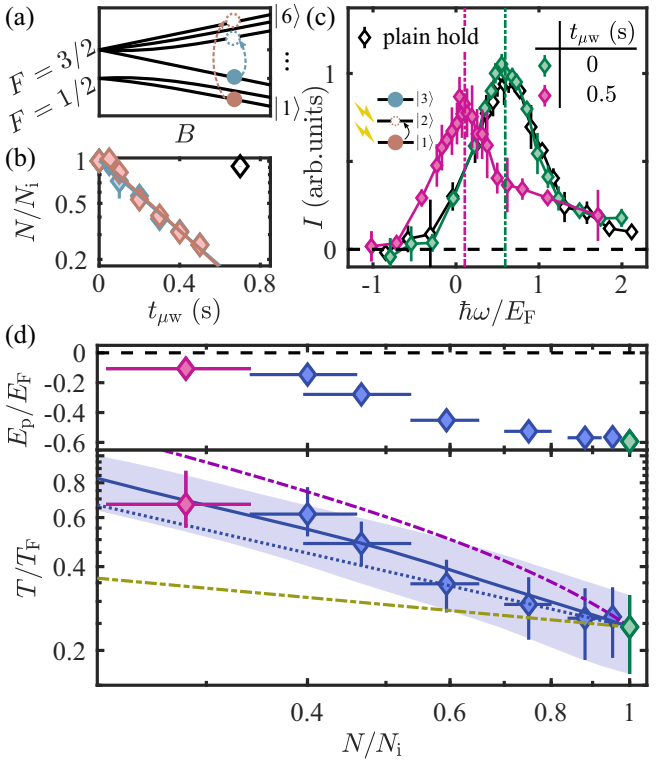

FIG. 3. Joule-Thomson effect of the unitary Fermi gas. (a) Breit-Rabi diagram of the ground state manifold of ^{6}Li (sketch not to scale). Solid (open) symbols represent the initial (final) states of the microwave transfer. (b) Microwave-driven decay of a unitary Fermi gas. Pink and blue diamonds are the populations in states $|1\rangle$ and $|3\rangle$ respectively. The black empty diamond shows the reference decay without microwave field. (c) Radio-frequency (rf) thermometry. The cartoon shows the internal states used in the rf spectroscopy: the gas, initially in a balanced mixture of $|1\rangle$–$|3\rangle$, is driven on the transition $|1\rangle \to |2\rangle$; the states that are imaged are marked with the lightning symbols. Green and magenta diamonds are the spectra at $t_{\mu w} = 0$ s and $t_{\mu w} = 0.5$ s, and black diamonds correspond to the spectrum after 0.7 s no-microwave hold. Dot-dashed vertical lines mark the peak response. (d) Degeneracy of a unitary Fermi gas during isenthalpic rarefaction. The peak frequency response E_p and T/T_F are shown along the rarefaction N/N_i, respectively in the upper and lower panel. The green and magenta diamonds correspond to the spectra in (c). The blue solid line is the prediction based on the EOS [27], fixing $(T/T_F)_i$ to the experimental values. The blue band is the uncertainty arising from the uncertainty on $(T/T_F)_i$. The dotted line shows the evolution of T/T_F at constant T. The purple (respectively yellow) dot-dashed line is the theoretical temperature evolution of an ideal Fermi (respectively Bose) gas during JT process; T_F is defined with the density of the corresponding (Bose or Fermi) gas.

timescale of the microwave-induced rarefaction is short, see [14].

For thermometry, we use radio-frequency (rf) spectroscopy and compare it to the calibrated spectra for the unitary gas as a function of temperature measured at MIT [28,29]. We transfer atoms from state $|1\rangle$ to state $|2\rangle$ and measure the transferred fraction as a function of ω, the detuning frequency relative to the bare $|1\rangle \to |2\rangle$ transition frequency (see Appendix C and [14]). Specifically, we extract the temperature from the peak response frequency $E_p \equiv -\hbar\omega_p$, whose magnitude decreases monotonically with increasing T/T_F [28].

We first verify that without microwave transfers and on the timescale of the experiment, evaporation and other T dynamics are negligible. We measure the initial rf spectrum of the gas [green diamonds in Fig. 3(c)] and after a hold of 0.7 s (black diamonds), without microwave field. The spectra are essentially identical; quantitatively, we extract $T/T_F = 0.24^{+7}_{-8}$ and $T/T_F = 0.23^{+7}_{-8}$ from $E_p = -0.59(2)E_F$ and $E_p = -0.61(2)E_F$, respectively.

When the microwave induces rarefaction, the rf spectra significantly change [see magenta diamonds in Fig. 3(c), corresponding to a rarefaction of $N/N_i = 0.28(6)$]. In fact, we observe that the magnitude of E_p/E_F continuously decreases with rarefaction [upper panel of Fig. 3(d)], indicating qualitatively that the quantum degeneracy decreases. In the lower panel of Fig. 3(d) we show the evolution of T/T_F in a unitary-gas JT process. For an initial condition $(T/T_F)_i = 0.24^{+7}_{-8}$ (blue diamonds), the data show that the unitary gas experiences a less pronounced heating compared to the ideal Fermi gas (purple dash-dotted line); the data are in very good agreement with the prediction based on the experimentally measured EOS (blue solid line) [27]. The band represents the uncertainty window arising from the uncertainty in $(T/T_F)_i$. We took an additional data set at a lower initial degeneracy, corresponding to $(T/T_F)_i = 0.35(4)$, and observe weaker heating (see [14] for details).

Despite the theoretical challenge in describing the strongly interacting Fermi gas, its JT effect is relatively simple to interpret in both the low-T ($T \ll T_c$) and high-T ($T \gg T_F$) limits. In the low-T limit, the unitary gas should exhibit a strong JT heating as $\theta_{JT} \propto -(T/T_F)^{-4}$ (which originates from both its nonvanishing ground state energy in the thermodynamic limit and its low-lying phononic excitations [30]). In the high-T limit, the unitary gas exhibits an effective interaction [$\propto -\log G(r)$] that is attractive [31]; it should thus cool during a JT process [14], akin to the ideal Bose gas. From the EOS, we expect that there exists an inversion temperature, i.e. the temperature at which the JT effect changes from heating to cooling, at $T_{inv} \approx 0.9T_F$. In the intermediate range of T/T_F explored in this work, we observe weak heating, in between the expectations for the ideal Bose and Fermi gases [yellow and purple dot-dashed lines in Fig. 3(d)].

In conclusion, we realized JT processes in the essentially ideal Fermi gas and the unitary Fermi gas by exploiting scale invariance and implementing u-constant rarefactions. In the range of temperature explored, we observed JT heating in both cases and the effect is lessened when the

repulsive quantum-statistical force is either weakened by the loss of degeneracy or counterbalanced by attractive interparticle forces.

In the future, it would be interesting to study the JT effect in other many-body platforms, such as dipolar gases [32], low-dimensional gases, and Hubbard systems [33,34]. The JT effect can encode interesting physics such as complex P-T diagrams delineated by boundaries called inversion curves—where μ_{JT} changes sign [35]. These diagrams are essentially unknown for strongly correlated quantum systems and they could provide valuable new information in settings where the interplay between interactions and quantum statistics is essential.

More specifically, it would be interesting to extend the study of the JT effect to the BEC-BCS crossover, where one expects a continuous transition from bosonic to fermionic behavior. It would be particularly intriguing to understand how the sign change of the JT effect at low T relates to the transition point where the nature of the single-particle excitations turns from bosonic to fermionic in the crossover (i.e. where $\mu(1/k_{\mathrm{F}}a) = 0$) [25]. While the absence of scale invariance poses interesting experimental challenges on how to realize a JT process in that system, the JT coefficient could also be extracted from the isothermal compressibility [14,27,36].

We thank Frédéric Chevy, Hadrien Kurkjian, Robert Smith, and Zoran Hadzibabic for comments on the manuscript. We thank Martin Zwierlein and Biswaroop Mukherjee for sharing their data. This work was supported by the NSF (Grants No. PHY-1945324 and No. PHY-2110303), DARPA (Grant No. W911NF2010090), the David and Lucile Packard Foundation, and the Alfred P. Sloan Foundation. G. L. S. acknowledges support from the NSF Graduate Research Fellowship Program.

Appendix A: Time-of-flight thermometry of a weakly interacting Fermi gas.—In our experiment, the gas parameter is small, $k_{\mathrm{F}}a \leq 0.02$, so interaction effects in flight are weak, i.e., the flights are essentially ballistic. Furthermore, $k_{\mathrm{F}}a$ is low enough so that interactions do not appreciably affect the *in situ* momentum distribution [14]; thermometry can thus be done as if the samples were noninteracting.

Appendix B: Microwave transfer.—We use a microwave field to transfer atoms from state $|1\rangle$ to $|6\rangle$, and from state $|3\rangle$ to $|4\rangle$, where $|j\rangle$ is the Zeeman sublevel labeled from the ground up ($j = 1, \ldots, 6$), see Fig. 3(a). The interactions of atoms in the final states with those in the initial states are very weak [37]. While the outcoupled states $|4\rangle$–$|6\rangle$ could inelastically collide and decay into either $|2\rangle$–$|6\rangle$ or $|1\rangle$–$|5\rangle$ [38], we see no evidence of deposited energy as a result of such processes. Furthermore, the absorption of the microwave photons is independent of the atoms' energy because the Doppler effect is negligible. The powers of the tones are adjusted so that the transfer rates on the two transitions are the same.

Appendix C: Radio-frequency (rf) thermometry of a unitary Fermi gas.—We apply a $t_{\mathrm{pulse}} = 2.5$ ms square rf pulse with a (single-particle) Rabi frequency $\Omega_0 = 2\pi \times 139(1)$ Hz to transfer a small fraction of atoms ($\leq$15%) from state $|1\rangle$ to state $|2\rangle$. The normalized response spectrum, $I(\hbar\omega/E_{\mathrm{F}}) = (N_2/N_1)E_{\mathrm{F}}/(\hbar\Omega_0^2 t_{\mathrm{pulse}})$ is temperature dependent (N_1 and N_2 are measured before and after the pulse, respectively). The bare $|1\rangle \rightarrow |2\rangle$ transition frequency is calibrated using a fully polarized sample prepared in state $|1\rangle$ [14].

*To whom all correspondence should be addressed: yunpeng.ji@yale.edu

[1] J. P. Joule and W. Thomson, London, Edinburgh, Dublin Philos. Mag. J. Sci. **4**, 481 (1852).
[2] C. Linde, Ber. Dtsch. Chem. Ges. **32**, 925 (1899).
[3] J. R. Roebuck, Proc. Natl. Acad. Sci. U.S.A. **12**, 55 (1926).
[4] J. O. Hirschfelder, R. B. Ewell, and J. R. Roebuck, J. Chem. Phys. **6**, 205 (1938).
[5] Ö. Ökcü and E. Aydıner, Eur. Phys. J. C **77**, 1 (2017).
[6] H. Ghaffarnejad, E. Yaraie, and M. Farsam, Int. J. Theor. Phys. **57**, 1671 (2018).
[7] J.-X. Mo, G.-Q. Li, S.-Q. Lan, and X.-B. Xu, Phys. Rev. D **98**, 124032 (2018).
[8] D. S. Kothari and B. N. Srivasava, Nature (London) **140**, 970 (1937).
[9] A. Einstein, Sitzungsber. Preuss. Akad. Wiss. Phys. Math. Kl. **1**, 3 (1925).
[10] E. Timmermans, Phys. Rev. Lett. **87**, 240403 (2001).
[11] T. F. Schmidutz, I. Gotlibovych, A. L. Gaunt, R. P. Smith, N. Navon, and Z. Hadzibabic, Phys. Rev. Lett. **112**, 040403 (2014).
[12] N. Navon, R. P. Smith, and Z. Hadzibabic, Nat. Phys. **17**, 1334 (2021).
[13] Y. Ji, G. L. Schumacher, G. G. T. Assumpção, J. Chen, J. T. Mäkinen, F. J. Vivanco, and N. Navon, Phys. Rev. Lett. **129**, 203402 (2022).
[14] See Supplemental Material at http://link.aps.org/supplemental/10.1103/PhysRevLett.132.153402 for details, which includes Refs. [15–19].
[15] T.-L. Ho and E. J. Mueller, Phys. Rev. Lett. **92**, 160404 (2004).
[16] X.-J. Liu, H. Hu, and P. D. Drummond, Phys. Rev. Lett. **102**, 160401 (2009).
[17] M. Li, L. Chen, and C. Chen, Phys. Rev. A **59**, 3109 (1999).
[18] M. M. Faruk and G. M. Bhuiyan, Acta Phys. Pol. B **46**, 2419 (2015).
[19] S. J. J. M. F. Kokkelmans (private communication).
[20] R. K. Pathria and P. D. Beale, *Statistical Mechanics*, 3rd ed. (Elsevier, New York, 2011).
[21] G. Uhlenbeck and L. Gropper, Phys. Rev. **41**, 79 (1932).
[22] W. J. Mullin and G. Blaylock, Am. J. Phys. **71**, 1223 (2003).

[23] The relation between the JT effect and two-body interactions can be quantitatively specified at the level of the second-order virial coefficient. Indeed, $\theta_{\mathrm{JT}} \propto b_2(T) - \frac{2}{5} b_2'(T)T$, where $b_2 = \int \mathrm{d}\mathbf{r_1}\mathrm{d}\mathbf{r_2}[1 - G(\mathbf{r_1}, \mathbf{r_2})]/(2V\eta\lambda_T^3)$.
[24] S. Tan, Ann. Phys. (N.Y.) **323**, 2987 (2008).
[25] W. Zwerger, *The BCS-BEC Crossover and the Unitary Fermi Gas* (Springer Science & Business Media, New York, 2011), Vol. 836.
[26] We observe that τ_{uni} saturates to a value shorter than τ_{vac} with increasing U_{box}, indicating that a loss mechanism other than evaporation is taking place.
[27] M. J. H. Ku, A. T. Sommer, L. W. Cheuk, and M. W. Zwierlein, Science **335**, 563 (2012).
[28] B. Mukherjee, P. B. Patel, Z. Yan, R. J. Fletcher, J. Struck, and M. W. Zwierlein, Phys. Rev. Lett. **122**, 203402 (2019).
[29] Z. Yan, P. B. Patel, B. Mukherjee, C. J. Vale, R. J. Fletcher, and M. Zwierlein, arXiv:2212.13752.
[30] For the ideal Fermi gas, $\theta_{\mathrm{JT}} \approx -(T/T_{\mathrm{F}})^{-2}$ in the low-T limit; the quadratic dependence stems from the particle-hole nature of the excitations.
[31] Unlike in ideal quantum gases, the origin of the effective high-T interaction potential of the unitary Fermi gas is not purely quantum statistical; it results from both the repulsive quantum-statistical force and the direct (effectively attractive) interatomic contact interaction.
[32] L. Chomaz, I. Ferrier-Barbut, F. Ferlaino, B. Laburthe-Tolra, B. L. Lev, and T. Pfau, Rep. Prog. Phys. **86**, 026401 (2022).
[33] I. Bloch, J. Dalibard, and S. Nascimbene, Nat. Phys. **8**, 267 (2012).
[34] C. Gross and W. S. Bakr, Nat. Phys. **17**, 1316 (2021).
[35] H. B. Callen, *Thermodynamics and an Introduction to Thermostatistics*, 2nd ed. (John Wiley & Sons, New York, 1985).
[36] B. Mukherjee, Homogeneous quantum gases: Strongly interacting fermions and rotating bosonic condensates, Ph.D. thesis, Massachusetts Institute of Technology, 2022.
[37] M. Lysebo and L. Veseth, Phys. Rev. A **79**, 062704 (2009).
[38] M. Houbiers, H. T. C. Stoof, W. I. McAlexander, and R. G. Hulet, Phys. Rev. A **57**, R1497 (1998).